Journal of Nonlinear and Convex Analysis
Volume 26, Number 7, 2025, 2345–2355

Yokohama Publishers
ISSN 1880-5221 ONLINE JOURNAL

AUTONOMOUS NAVIGATION FOR 4 WHEEL SHUTTLE VEHICLE IN THE NARROW AREA UNDER THE VISUAL SIMULTANEOUS LOCALIZATION AND MAPPING(VSLAM) METHOD

HEONJONG YOO AND SEONGGON CHOI*

Abstract. Visual simultaneous localization and mapping at the narrow standing still obstacle area based on the precise map facilitates the 4 wheel shuttle vehicle to recognize its current longitude and latitude information and heading angle while moving at the aforementioned environment effectively. In the broad notion, trajectory tracking control including waypoint following method is cruicial techniques that facilitates a 4 wheel shuttle vehicle's fully driving performance without human's intervention. The Laptop for MATLAB and for Ubuntu is a high- and low-level control system that influences the 4 wheel shuttle vehicle equipped with the Inertial Measurement Unit(IMU), 16 channels LiDAR, and Encoder Sensors of the 4 wheel shuttle vehicle. The 4 wheel shuttle vehicle is controlled in terms of a Robot Operating System (ROS) connection, set-up parameters for each 4 wheels, and visualizes sensor data in a MATLAB odometry system. In the paper, the proposed model presents more accurate path following scenario that integrates the visual simultaneous localization and mapping(VSLAM) algorithm with the 4 wheel shuttle vehicle. The generated reference path following scenario that performs optimal navigation and standing still object avoidance performance successfully localized 4 wheel shuttle vehicle simultaneously and it is tested at the narrow stading still obstacle area. The Root mean square error(RMSE) between generated reference path and actual path is demonstrated through several experimental results in the ROS map. In this presentation, the visual simultaneous localization and mapping(VSLAM) method is applied for 4 wheel independent mobile platform, and it is shown that the result is effective way to move in a safe way especially in the narrow indoor environment. The root mean square error(RMSE) is about 3 and 4 centimeter which shows better performance than Lidar odometry and mapping(LOAM) method.

1. Introduction

Today, the Robot operating system (ROS) API will take advantage of modern libraries utilized in commercial mobile robot systems for robot manipulators, autonomous agriculture mobile robots. Furthermore, autonomous ground vehicles (AGVs) applications such as outdoor and indoor mobile robots, cleaning robots,

2020 *Mathematics Subject Classification.* 93C40.

Key words and phrases. Lidar mapping, visual simultaneous localization and mapping(VSLAM), optimal path following simuataneously.

This work was partly supported by the MSIT (Ministry of Science and ICT), Korea, under the Grand Information Technology Research Center support program (IITP-2025-RS-2020-II201462, 50 %) supervised by the IITP (Institute for Information & communications Technology Planning & Evaluation) and Basic Science Research Program through the National Research Foundation of Korea (NRF) funded by the Ministry of Education (No. RS-2020-NR049604, 50 %).

*Corresponding author.

security robots, vehicles, military, and industry of their industrial robotics. The industries used robot operating systems (ROS) toolboxes to control their application of robotic arms, medical-surgical robots, logistics mobile robots, manufacturing robots, agriculture robots, healthcare logistic robots and service robots.

The accuracy of the mobile vehicle autonomous location system is critical for efficient and safe navigation. The Global Navigation Satellite System (GNSS) is used worldwide to recognize of the current position and navigation of the 4 wheel shuttle vehicle [6]. The trajectory tracking method represents the current position of 4 wheel shuttle vehicle and reaches the goal of accerelating commands. In the final demo, we start with the starting points where we developed the kinematic model and odometry for the mobile robot path following the model into a single Simulink environment that can move the mobile robot. Therefore, the precision of the recognizating the current longitude and latitude information of the 4 wheel shuttle vehicle was implemented based on the available constellation and the well-shaping of the linear and angular velocities input [16]. The map acquisition shows how to acquire data from the mobile robot regarding the environments to match the data to obtain a complete map. The VSLAM method is a recursive estimation procedure that simultaneously minimizes: the localization errors of the 4 wheel shuttle vehicle and the narrow area mapping errors [24]. The SLAM algorithm was proposed in [7]. SLAM methods have been implemented for autonomous mobile robots [10]. The waypoint-following control is one of a path-following method that computes the mobile robot's input commands to move the 4 wheel shuttle vehicle from the starting point to the look-ahead position. However, the autonomous mobile robot uses Global Positioning Systems (GPS) and inertial measurements to navigate, as described in [20]. The robot state estimate accumulates drift during long traversals. This issued loop closure localization, which recognizes revisited sites using either visual SLAM or LiDAR methods for a mobile robot position known by the position information of the x, y, θ, and segment-based algorithms such as seg Match are used in LiDAR approaches to recognize localizations [14]. The perception of the state of agricultural machinery and information about the environment is attracting more interest from researchers [7]. The pure pursuit control will generate the control action of the two linear and angular velocities input $V(t)$ and $W(t)$ in [20]. Stereo vision and 3D LiDAR independently detect barriers, which are then combined in uncertainty to produce final classification results that generate a path that accounts for the obstacle on the map [5]. However, finding a path sequence of points that go from the starting to the end point of a new mobile robot position and 4 wheel shuttle vehicle's actual path is decided by the path generation defined by the way-points, and the standing still obstacle on the mobile robot's path. The popular positioning system of the Global Navigation Satellite System (GNSS) does not perform well in indoor environments. A precise positioning and localization system for autonomous mobile robots have required precision for narrow indoor area with standing still separated obstacle; with a centimeter precision, all described in [13]. This map operation continues until the map is dense enough for the purpose. SLAM stands for localization and mapping of 4 wheel shuttle vehicle simultaneously. It is a task to estimate a ROS map of the area and at the same time recognize the current position of the mobile robot. However, the mobile robot needs a map to move in a safe way

within unknown environments. The 4 wheel shuttle vehicle needs to build a map of the area to localize itself within that mapping. Several researchers were researching autonomous indoor positioning systems using the Global Positioning System (GPS) which cannot be used successfully in the indoor environment. They investigate a variety of systems capable of centimeter accuracy, including a tachometer, cameras, Radio Frequency Identification (RFID), magnetic systems, ultrawideband (UWB), and sound [3]. The current state-of-the-art laser scanning of the Simultaneous Localization and Mapping (SLAM) system is a constant velocity model. Therefore, the Gaussian algorithm procedure is required to implement the motion model. The PRM is a probabilistic road map, mainly considered in two phases. The first phase of the image construction on the right side builds up a graph that links different positions and different free positions inside the map [11]. The second phase search was for a specific mobile robot path that connected lined one point with another point. Specifically, the construction phase consists of three steps. It starts from the map course to check some random robot points. The cardinality of these random points depends on how to define the problem. An example is a low-density problem that selects a point each time on the map. On the other side of research, trajectory tracking control method is applied for 4 wheel independent steering system in [18]. [19] says that a novel differential drive assisted steering technology is applied for the independent-wheel-drive electric vehicle, and compares the result with the traditional PID controller in which the proposed method shows better performance.In [4], a nonlinear disturbance observer and sliding mode controller is applied for the hardware-in-the-loop system, which can achieve better tracking performance and suppress the chattering phenomenon. [9] proposed artificial potential field that is applied to the framework of automated vehicles. Specifically speaking for AI, the deep reinforcement learning technique is studied in [15]. [2] shows recent Deep Deterministic Policy Gradient(DDPG) algorithm can be used for path following of bicycle type model in mobile platform. Furthermore, the Deep Deterministic Policy Gradient(DDPG) method can also be applied for 3D path-following such as drone's control in [23]. With the aforementioned development, the author previously developed waypoint following mechanism which is incorporated into ROS publish and subscribe system to control 4 wheel mobile platform described in [8]. [1] shows that dynamic obstacle avoidance and path following is implemented through reinforcement learning using the mobile platform.

Recently, several autonomous trajectory generation algorithm is proposed, in [17], which utilizes convex optimization algorithm. For drone's path -following, the [21] offered autonomous drone avionics amplified with pontryagin-based optimization to improve robotic drone path following. Furthermore, [12] proposed autonomous trajectory shaping for noise amelioration in robotics illustrating sinusoidally shaped trajectories yield the best trajectory tracking ability.

In this presentation, proposed model produces a simultaneous localization and mapping and generated reference path following scenario that incorporate ROS map with 4 wheel shuttle vehicle using the ROS Simulink program. The trajectory tracking problem that implement optimal VSLAM navigation and standing still obstacle avoidance performance shows that the vehicle which recognizes it's current longitude

and latitude information is tested at the narrow area. The improvement of accuracy is shown through Root mean square error. We implemented the path-following algorithm with our real 4 wheel shuttle vehicle and compared the accuracy between the LiDAR odometry and VSLAM method. In this method, an environment of SLAM may be generated and updated automatically during robot navigation. We optimized the accuracy of the SLAM algorithm for the recognization of the current position of 4 wheel shuttle vehicle.

2. Setup parameters of mobile robot 3D, ROS RVIZ (ROS visualization) Simulink, and ROS Gazebo

The mobile robot parameters set up to the differential drive 4 wheel shuttle vehicle's longitude and latitude represented the linear speed input and angular velocity input that presents 4 wheel shuttle vehicle's angular speed. The orientation data $y = v \times \sin(\theta)$ is the variation of x in the y direction and the opposite for $y = v \times \sin(\theta)$ of the mobile robot direction. In the final step, the $W(t)$ is simply the derivative of the mobile robot's heading angle θ. Equation (3.1) produces the information on the derivative $x(t), y(t)$ position of shuttle vehicle. However, the Inertial Measurement Unit (IMU) and encoder worked with the sampling frequencies are 200 and 100 cycles per second (HZ) and used the mobile robot's reference coordinate for the ground robot's position at the time step i during the encoder's time cycle. In Fig. $1(a)$, the mobile vehicle's placement at the next time-step j is shown by the trajectory of the robot, c_{ij} and the chord-length vector L_{ij} Eq (2.1).

$$L_{ij} = \begin{bmatrix} I_{ij} \\ \delta\theta_{yaw} \\ \delta\theta_{pitch} \end{bmatrix}. \tag{2.1}$$

Where L_{ij} is the vector length. The mobile robot parameters set up $t\delta\theta_{pitch}$ and $\delta\theta_{yaw}$ are robot pitch and yaw variations. Using the current Inertial Measurement Unit (IMU) measurement and bias, we can determine $\delta\theta_{pitch}$ and $\delta\theta_{yaw}$ variations.

We used the encoder's estimated angle to compute the distance of the trajectory c_{ij} by applying Eq (2.2). By calibrating the odometry's intrinsic parameter matrix j, it is possible to derive chord length L_{ij} by geometric reasoning and approximation because the robot's rotation is modest within the sample interval $(0.6ms)$.

$$l_{ij} = o_{ij} \cos(c \times \delta\theta_{yaw}), \tag{2.2}$$

$$DP_{o_i o_j} = \begin{bmatrix} c_{ij} \cos(c \times \delta\theta_{yaw}) \cos(\delta\theta_{pitch}) \cos(\delta\theta_{yaw}) \\ c_{ij} \cos(c \times \delta\theta_{yaw}) \cos(\delta\theta_{pitch}) \sin(\delta\theta_{yaw}) \\ -c_{ij} \cos(c \times \delta\theta_{yaw}) \sin(\delta\theta_{pitch}) \end{bmatrix}. \tag{2.3}$$

Where c_{ij} is the length of the trajectory curve c_{ij} and c is used for the ground roughness to compensate for mistakes caused by minor ground variation. In this case, the minimum surface roughness is 1 which corresponds to a smooth surface. According to the actual working environment of the mobile robot and the ground's roughness can also be adjusted. To obtain the position variation from time-step j to time-step i. We finally project the motion vector onto the O_i, O_j coordinate system. The mobile robot used rotate matrix equation. The radius model transforms the speed command and the linear and angular speed command into the angular

speed of each mobile robot wheel. The odometry is the transformation from the speed of the mobile robot into the position described in Fig. 1(b). The mobile robot kinematic model transformed the linear and angular speed command to this information. The first step is to take the command velocity $cmd_{velocity}$ into the velocities input transform. This transformation is a kinematic transform based on the reference speed for the mobile robot's right wheel $V_{reference\ right}$ will be the actual linear speed of the mobile robot in addition to $[W(t)]$ which are the mobile robot angular speed produced by Eq. (2.3).

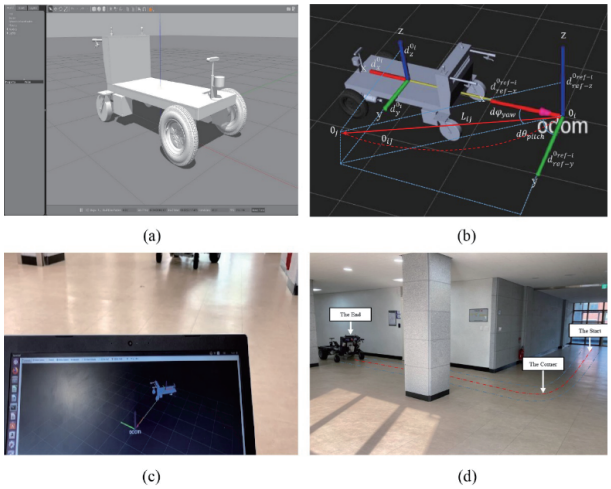

FIGURE 1. The 3D indoor mobile robot to precisely register in the corridor and localize with ROS Gazebo Simulink (a). Set up mobile robot odometer model (b). The result of ROS RVIZ Simulink with a real mobile robot (c). The mobile robot experimental setup indoor environment (d).

3. The mobile robot kinematic model, odometry, and inertial measurement unit (IMU)

We selected the unicycle model for the experimental test since it is well-known type of 4 wheel vehicle in many industrial field, such as floor clearning, and wheelchair robot.

The 4 wheel shuttle vehicle has one input and two outputs, so the inputs are the speed command that we want the robot to achieve. The outputs are the Velodyne LiDAR sensor result and the wheel commands measured from the encoders inside the 4 wheel shuttle vehicle wheels.

The right side of the 4 wheel shuttle vehicle $wheel_{velocity}$ wheel left, wheel right is the output of the speed command, and the left side of wheel $cmd_{velocity}$ wheel left, wheel right is the input of the speed command. Both are measured from the mobile robot speed Eq (3.1), (3.2), (3.4). This transformation model is produced from the linear and angular speed $V(t)$, $W(t)$ to the speed of each wheel. The mobile robot's right and left are linear speeds that transform this speed into the corresponding

rotational speed. It is sufficient to divide each of the mobile robots into the speed of the right and left wheels by radius R.

$$\begin{bmatrix} \dot{X}(t) \\ \dot{Y}(t) \\ \dot{\theta}(t) \end{bmatrix} = \begin{bmatrix} \cos(\theta) & 0 \\ 0 & \sin(\theta) \\ 0 & 1 \end{bmatrix} \begin{bmatrix} V(t) \\ W(t) \end{bmatrix}. \tag{3.1}$$

The integrated form for (3.1) are given as

$$X(t) = \int_0^t \cos(\theta(t))V(t)dt, \tag{3.2}$$

$$Y(t) = \int_0^t \sin(\theta(t))V(t)dt, \tag{3.3}$$

$$x(t) = \int_0^t W(t)dt. \tag{3.4}$$

In the first step, the mobile robot path must be 2 if the trajectory $K > K_{\max}$, is not trackable. If $K > K_{\min} \rightarrow W_{\max}V_{\max}$ defined in (3.6), there will always be a sufficient rotation speed condition for the input of linear and angular speed to control the expected curvature to maintain. Hence, the maximum of the linear speed of the mobile robot $V_{\max}$ is utilized for the definition of V_i, and the rotational speed definition of W_i,determined by $W_i = K_{\min} \cdot V_{\max}$ in Eq (3.5)-(3.7).

$$\int_0^{\delta t_i} V_i \cos(\theta_i + W_i t)dt = X_{i+1} - X_i = \delta X_i, \tag{3.5}$$

$$\delta X_i = \frac{V_i}{W_i} \sin(\theta_i + W_i t)]_0^{\delta t_i} = \frac{\sin(\theta_i + W_i \delta t_i) - \sin(\theta_i)}{K_i}, \tag{3.6}$$

$$\delta t_i = \frac{\sin^{-1}(\delta x_i \dot{k}_i + \sin(\theta_i)) - \theta_i}{W_i}. \tag{3.7}$$

Secondly. the time dimension to V_i and W_i is assigned and then the user transforms the aforementioned variables V_i,W_i into $V_i(t)$ and $W_i(t)$. The model was determining a series of δt_i between all P_i. In the SIMULINK, the small time constant represents the sampling time in P_i and next sample P_{i+1} on the path, assuming that it is constant within this short time interval. Based on the aforementioned fact, the following equations (3.5)-(3.7) will hold, [22]. The determination of the spatial variables V_i and W_i in SIMULINK is implemented by the curvatures K at each point along the path.

4. To calculate the result by using RMSE equations

To evaluate the various matching sets of the ROS map, the real-world odometry data sets to the ROS map registration was performed by taking into account the point cloud data received from the mobile robot Velodyne HDL-16 LiDAR sensor and odometry sensors of the mobile robot. The total root mean square error (RMSE) and the translational, and rotational errors is provided by comparing with

the actual data from ROS odometry block. As shown below, the RMSE describes in Eq. (4.1) by point j ([22]).

$$RMSE = \sqrt{\frac{1}{N}\sum_{j=1}^{n}(T_j - RS_j - t_r)^2}. \tag{4.1}$$

Where T, S, R and t_r denote the source point cloud, the target point cloud, and the rotation and translation transformations.

5. Results and discussion

5.1. **The test mobile robot moved along the indoor environment at four travel speeds.** Using simultaneous localization and mapping (SLAM), the 4 wheel shuttle vehicle knows its current longitude and latitude information at the indoor area while moving and estimated x and y positions on the 2D map. We used a LiDAR sensor to estimate the position of the 4 wheel shuttle vehicle, and further estimate the heading angle from IMU sensor in the unknown environment and to build at the same time a $2D$ map of this environment. SLAM is the task of estimating an environmental map while simultaneously localizing the sensor to the mobile robot. The 4 wheel shuttle vehicle needs a ROS map for navigation in unknown environments. The 4 wheel shuttle vehicle must produced a ROS map of the narrow area and localize the platform within it. Furthermore, it requires the pole to estimate the obstacle by using the map. Therefore, the role of SLAM is to estimate anytime to the trajectory of the LiDAR sensor to extract the key points from the current frame in the map described in Fig. 2.

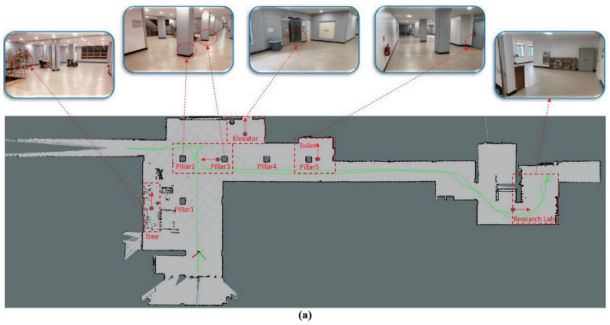

Figure 2. The generated the 2D SLAM using the Velodyne VLP-16 (PUCK) LiDAR mounted on the mobile robot (a). The mobile robot used lidar data and IMU data to precisely register in the mobile robot localization and optimization by reducing the uncertainty in indoor environments (b).

5.2. **Evaluation of LiDAR mapping and LiDAR odometry using SLAM algorithms.** We investigated and evaluated the SLAM algorithm LOAM (LIDAR, IMU) and evaluated the location of our model's mobile robot using ORB SLAM in indoor environments, both of which hold some of the top scores on the dataset

benchmarks. The developed localization algorithm shows approximately the same behavior for all paths, with slight differences in RMS errors described in Table 1. From between straight lines and turning movements, we obtained the accuracy results of the robot from Table 2. Our mobile robot's localization had to be accurate relative to starting point of the 4 wheel shuttle vehicle. Furthermore, the user estimate the position of the 4 wheel shuttle vehicle in the operational indoor environment using ROS map in Fig. 3, 4.

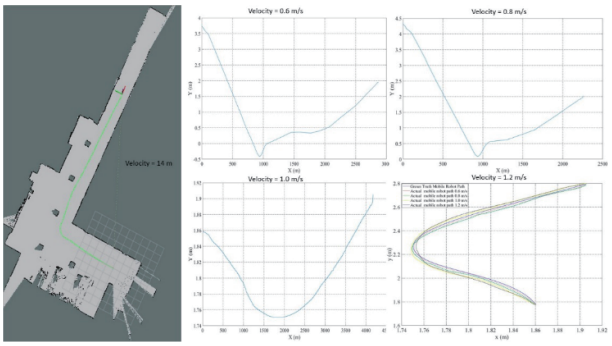

FIGURE 3. The comparison between reference path and actual path, and estimated linear and angular velocities in the narrow indoor environment in the Experiment 1.

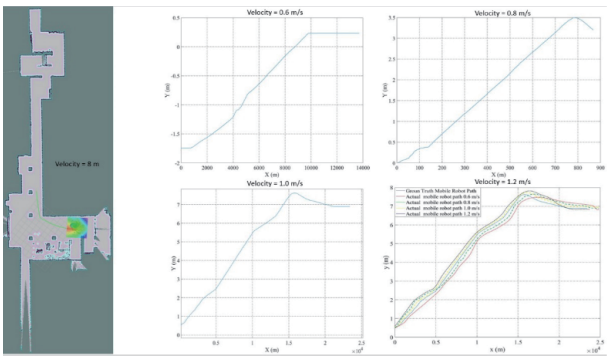

FIGURE 4. The comparison between reference path and actual path, and estimated linear and angular velocities in the narrow indoor environment in the Experiment 2.

Fig. 5 shows the 2D map we generated using the SLAM. The RMSE(Root mean square error) calculated from (4.1) is given as Table 1. The RMSE between the generated reference path and the actual path is small in which 4 wheel mobile platform moves to the designated position in a safe way.

The developed localization algorithm shows approximately the same behavior for all paths, with slight differences in RMS errors. From between straight lines and turning movements, we obtained the accuracy results of the robot from Table 1.

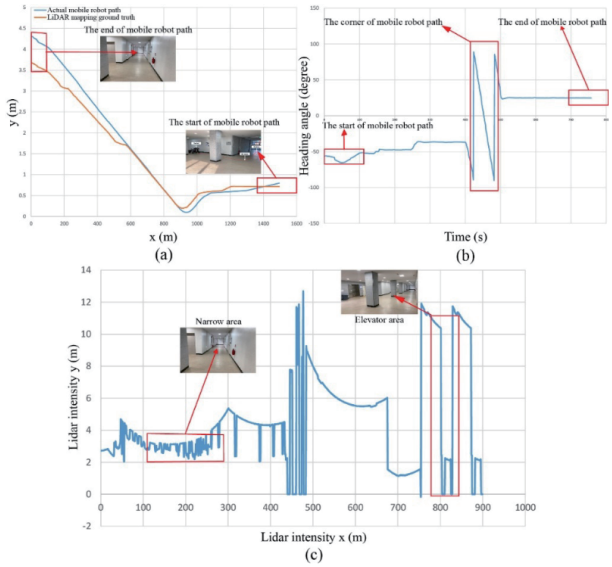

FIGURE 5. Generated the 2D SLAM using the 16 channel (PUCK) LiDAR and mounted it on the 4 wheel shuttle vehicle (a). The 4 wheel shuttle vehicle used lidar data and IMU data to precisely register in the mobile robot localization and optimization by reducing the uncertainty in indoor environments (b).

TABLE 1. The Root mean square error for indoor experiment in Figures 3 and 4

LOAM in Figure 3	Proposed method in Figure 3
6 cm	3 cm
LOAM in Figure 4	Proposed method in Figure 4
7 cm	4 cm

The mobile robot localization algorithm developed uses the starting point IMU data to calibrate the coordinate system, which all mobile robot path planning converts into simple 2D coordinates for positional purposes. We evaluated the different results of the RMSE of the longitude and latitude information of the 4 wheel shuttle vehicle. The solution for LiDAR mapping and LiDAR odometry required the tool with centimeter precision in a sparse operational indoor environment.

6. DISCUSSION

We developed the kinematic model (Kinematic ($cmd_{velocity}$) VW) and this kinematic transforms the speed command input $V(t), W(t)$ into the reference of a mobile robot left and right. This kinematic module is used in both the input and output ports. The Wheel Velocity measured $wheel_{left} wheel_{right}$, those measured the speed of the left and right wheels of the 4 wheel shuttle vehicle. The output kinematic $V_m W_m$ and $cmd_{velocity}$ is measured by the linear and velocity speed measured. The

odometry represents the actual speed measured by the mobile robot to extract the longitude and latitude information. Lastly, the generated reference following module is provided. Furthermore, the module takes the position of the mobile robot and compares it with a path that follows the input in this block and produces a speed from $V(t)W(t)$, the command speed that forces the 4 wheel shuttle vehicle to pursue the generated reference path using generated velocities speed input. The advantage of proposed method is that the accuracy was improved compared to the existing design method. The shortcoming of proposed method was that there was possibility of touching dynamical obstacle such as human, and moving object that suddenly interrupted to the mobile platform. In the future, some of mechanism should be incorporated into the proposed algorithm for the possibility of moving object-aware scenario.

7. Conclusion

In addition to the significant amount of polish needed for production, a revised construction, obstacle avoidance, and a fully automated workflow should be implemented to improve the robot. A SLAM algorithm that fuses the output from all three sensor types (IMU, LIDAR, and cameras) may also be required. Our proof-of-concept prototype convinced the stakeholders that the project has potential. The project is currently being expanded upon by Automation AB, which hopes to release a full-featured product in the future. We presented our local and mapping systems that use an efficient 3D model

References

[1] K. Almazrouei, I. Kamel and T. Rabie, *Dynamic obstacle avoidance and path planning through reinforcement learning*, Applied Science **13** (2023): 8174.

[2] Y. Cao, K. Ni, X. Jiang, T. Kuroiwa, H. Zhang, T. Kawaguchi, S. Hashimoto and W. Jiang, *Path following for autonomous ground vehicle using DDPG algorithm: A reinforcement learning approach*, Applied Science **13** (2023): 6847.

[3] F. Che, Q. Z. Ahmed, P. I. Lazaridis, P. Surrephong and T. Alade *Indoor positioning system (IPS) using ultra-wide bandwidth (UWB)—For industrial internet of things (IIoT)*, Sensors **23** (2023): 5710.

[4] J. Chen, Z. Shuai, H. Zhang and W. Zhao, *Path following control of autonomous four-wheel-independent-drive electric vehicles via second-order sliding mode and nonlinear disturbance observer techniques*, IEEE Transactions on Industrial Electronics **68** (2021), 2460–2469.

[5] J. Duan, Y. Huang, Y. Wang, X. Ye and H. Yang, *Multipath-closure calibration of stereo camera and 3D LiDAR combined with multiple constraints*, remote sensing **16** (2024): 258.

[6] D. Eredits, R. Krecht and N. Boros, *GPS based navigation and mobile base station of a mobile robot platform*, Chemical Engineering Transactions **107** (2023), 385–390.

[7] Y. Fei, Y. Zhuang, Q. Zhao, G. Liao and Q. Fu, *Development of an intelligent monitoring system for agricultural machinery*, in: 019 3rd International Conference on Robotics and Automation Sciences (ICRAS), Wuhan, China, 2019, pp. 161–165.

[8] M. H. Hong, H. J. Yoo and S. G. Choi, *Incorporation of waypoint following logic into ROS publish and subscribe mechanism*, in: Proceedings of 2024 26th International conference on Advanced Communication Technology(ICACT), IEEE, 2024, pp. 373–375.

[9] Y. Huang, H. Ding and Y. Zhang, *A motion planning and tracking framework for autonomous vehicles based on artificial potential field elaborated resistance network approach*, IEEE Transactions on Industrial Electronics **67** (2020), 1376–1386.

[10] K. B. Kis, J. Csempesz and B. C. Csáji, *A simultaneous localization and mapping algorithm for sensors with low sampling rate and its application to autonomous mobile robots*, Procedia Manufacturing **54** (2021), 154–159.
[11] H. Korrapati, *Loop closure for topological mapping and navigation with omnidirectional images*, Universite Blaise Pascal, Doctoral Dissertation, 2013, pp. 1–147.
[12] E. Kuck and T. Sands, *Sapce robot sensor noise amelioration using trajectory shaping*, Sensors **24** (2024): 666,
[13] G. Lachapelle, *GNSS indoor location technologies*, Journal of Global Positioning Systems **3** (2004), 2–11.
[14] Y. Liu, H. Wu, Y. Wei, M. Ren and C. Zhao, *Improved LiDAR localization method for mobile robots based on multi-sensing*, remote sensing **14** (2022): 6133.
[15] S. S. Mousavi, M. Schukat and E. Howley, *A deep reinforcement learning: An overview*, in :Proceedings of SAI Intelligent Systems Conference (IntelliSys), IEEE, 2017, pp. 426–440.
[16] E. Rubies and J. Palacin, *Defining the consistent velocity of omnidirectional mobile platforms*, Machines **12** (2024): 397.
[17] A. Sandberg and T. Sands, *Autonomous trajectory generation algorithms for spacecraft slew maneuvers*, Aerospace **9** (2022): 135.
[18] Y. Tong, H. Jing, B. Kuang, G. Wang, F. Liu and Z. Yang, *Trajectory tracking control for four-wheel independently driven electric vehicle based on model predictive control and sliding model control*, in: Proceedings of 5th CAA International Conference on Vehicular Control and Intelligence (CVCI), IEEE, 2021, pp. 1–5.
[19] J. Wang, T. Yan, Y. Bai, Z. Luo, X. Li and B. yang, *Assistance quality analysis and robust control of electric vehicle with differential drive assisted steering system*, IEEE Access **8** (2020), 136327–136339.
[20] R. Wang, Y. Li, J. H. Fan, T. Wang and X. Chen, *A novel pure pursuit algorithm for autonomous vehicles based on salp swarm algorithm and velocity controller*, IEEE Access **8** (2020), 166525–166540.
[21] J. Xu and T. Sands, *Autonomous drone electronics amplified with pontryagin-based optimization*, Electronics **12** (2023): 2541.
[22] H. J. Yoo and S. G. Choi, *Navigation path following platform for a greenhouse shuttle robot using the state - flow method*, Mathematical Problems in Engineering **2024** (2024): 8810990.
[23] Y. Zheng, J. Tao, Q. Sun, X. Zheng, H. Sun, M. Sun and Z. Chen, *DDPG-based active disturbance rejection 3D path-following control for powered parafoil under wind disturbances*, Nonlinear Dynamics **111** (2023), 11205–11221.
[24] A. Zureiki and M. Devy, *SLAM and data fusion from visual landmarks and 3D planes*, The International Federation of Automatic Control **41** (2008), 14651–14656.

Manuscript received October 7, 2024
revised December 20, 2024

Heonjong Yoo
Research Institute for Computer and Information Communication(RICIC), Chungbuk National University, Cheongju-city, Republic of Korea
E-mail address: 622061@chungbuk.ac.kr

Seonggon Choi
Information and Communication Engineering,Chungbuk National University, Cheongju-city, Republic of Korea
E-mail address: sgchoi@chungbuk.ac.kr